

Article

Ti-Doped Pd-Au Catalysts for One-Pot Hydrogenation and Ring Opening of Furfural

Nandan Shreehari Date ¹, Valeria La Parola ² , Chandrashekhar Vasant Rode ¹ and Maria Luisa Testa ^{2,*} 

¹ Chemical Engineering and Process Development Division, CSIR-National Chemical Laboratory, Dr. Homi Bhabha Road, Pashan, Pune 411008, India; ndate.2799@gmail.com (N.S.D.); cv.rode@ncl.res.in (C.V.R.)

² Institute for the Study of Nanostructured Materials (ISMN)-CNR, via Ugo La Malfa 153, I-90146 Palermo, Italy; valeria.laparola@cnr.it

* Correspondence: marialuisa.testa@cnr.it; Tel.: +39-091-680-9253

Received: 23 May 2018; Accepted: 14 June 2018; Published: 20 June 2018



Abstract: Pd-Au bimetallic catalysts with different Pd/Au atomic ratios, supported on ordered structured silica (Hexagonal mesoporous silica—HMS, or Santa Barbara Amorphous-15—SBA-15) were evaluated for one-pot hydrogenation of furfural to 1,2-pentanediol. The surface and structural properties of the catalysts were deeply investigated by X-ray photoelectron spectroscopy (XPS), X-ray diffraction (XRD), N₂ adsorption isotherms (BET), Infrared spectroscopy (IR), and acid capacity measurements. XPS studies revealed that Ti doped supports had higher dispersion of the active phase, particularly in the case of Pd-Au materials in which Ti played an important role in stabilizing the metallic species. Among the various process conditions studied, such as temperature (160 °C), catalyst amount (10% *w/w*), and reaction time (5 h), H₂ pressure (500 psi) was found to improve the 1,2-pentanediol selectivity. The SBA silica bimetallic Ti-doped system showed the best performance in terms of stability and reusability, after multiple cycles. Under specific reaction conditions, the synergism between Pd-Au alloy and Ti doping of the support allowed the ring opening pathway towards the formation of 1,2-pentanediol in furfural hydrogenation.

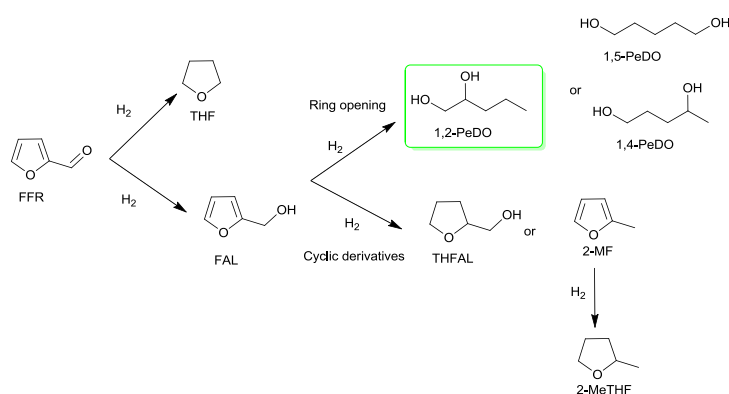
Keywords: hydrogenation; ring-opening; bimetallic catalyst; furfural

1. Introduction

In recent years, the biomass as a renewable feedstock has been gaining utmost importance in order to meet the global need for fuels and chemicals from sustainability perspectives [1,2]. Biomass derived from the lignocellulose part is rich in carbohydrates and furan derivatives, and the presence of oxygen in their structure makes them suitable for further utilization to obtain added-value products. The research addressing the development of new catalysts for achieving target products in a one-step reaction is the key task not only to decrease the processing cost but also to improve the sustainability potential of the industrial processes [3–6].

Furfural (FFR), obtained by the selective acid catalyzed dehydration of naturally available arabinose and xylose, is considered one of the 12 main platform molecules [6,7]. FFR can be selectively transformed into different furanic compounds [7–9] and polyols [10–15] which have wide range of commercial and industrial applications (Scheme 1). The selective conversion of FFR into open chain compounds as alcohol or diols received much attention in the last few years due to their wide range of applications in polymer industries for the production of polyester and polyurethanes [16–18], as well as for the synthesis of fungicides, disinfectants, and fine chemicals. New green strategies for the production of valuable polyols from biomass are highly desirable, as well as the development of

multifunctional catalytic systems for the one-pot conversion of FFR with a switchable selectivity to 1,2-pentanediol (1,2-PeDO) [16]. The conventional route for the synthesis of 1,2-PeDO is based on petroleum stock involving a multistep process, starting from alkene derivative that undergoes epoxidation and subsequent hydrolysis to give 1,2-PeDO using mineral acids such as H_2SO_4 , HCl , etc. [17]. Several homogeneous catalytic systems have been explored for the transformation of furfural into 1,2-PeDO using peroxides and per-carboxylic acids [18–20]. Efforts are being made to turn the process into “green” chemical reaction working on the procedures (reagent ratio or catalyst amount) and the heterogenous catalytic materials. In fact, the use of solid catalyst is indeed very favorable from a sustainable point of view, due to its simple separation, regeneration, and recycling of the material for different cycles [21,22]. This implies a high efficiency of the materials accompanied by a decrease in the processing cost.



Scheme 1. Furfural (FFR) Hydrogenation products.

Recently, different monometallic Pd-based materials were deeply studied for furfural hydrogenation. Palladium nanoparticles were deposited on various supports, such as carbon [23,24], SBA-15 silica [25], alumina [23], titania [26], and zeolite [27], showing good performance for the selective hydrogenation of FFR. It is important to notice that, in all cases, different hydrogenated derivatives were obtained, but FFR ring-opening for achieving the formation of polyols did not occur in any case. As far as the bimetallic catalytic systems are concerned, very few studies have been reported for the one-pot conversion of furfural to added value products. The use of copper-nickel catalysts supported on alumina [28] showed that Cu/Ni ratio and temperature play a significant role in the products distribution. In none of these reports, the selectivity to pentanediols could be achieved as furfuryl alcohol (FAL) and 2-methylfuran (2-MF) were formed. Yang et al. explored the selective hydrodeoxygenation of 5-hydroxymethylfurfural (5-HMF) on $RuMoO_x/C$ catalyst [29]. It was shown that the synergistic effect between the metallic Ru and acidic MoO_x species resulted in a high selectivity to 2,5-dimethylfuran (DMF) without formation of any diols. The bimetallic system of Pd-Ir supported on silica gave complete conversion of furfural with a high selectivity towards tetrahydrofurfuryl alcohol (THFAL) and FAL [30]. Improving the catalyst performance by addition of a third metal ($PdIrReO_x/SiO_2$), the same authors achieved one-pot selective conversion of furfural to 1,5-PeDO [31]. Recently, the Ni-Co/SBA-15 catalytic system [32] has shown good performance for the preparation of THFAL, confirming, once again, that the achievement of polyols still remain a challenge. Pd-Au nanoparticles supported on carbon or graphitized carbon showed an excellent performance in the selective hydrogenation of biomass-derived 5-hydroxymethylfurfural (HMF) to obtain DMF; nevertheless, small quantities of hexanediols were also formed [33,34]. Different studies on the efficiency of Pd-Au materials suggest that the bimetallic form was more active than the monometallic one, due to the formation of an alloy and the synergistic effect of both metals in the reaction mechanism [35–37]. The addition of gold improves the efficiency of palladium-based catalysts also in the selective hydrogenation of unsaturated C=C bonds in aromatic-containing platform

molecules [38]. Moreover, among various supports (C, Al₂O₃, and SiO₂), when bimetallic system on high surface area silica was used, a further beneficial influence was observed due to a better dispersion of metal nanoparticles. Recently, we have studied different mono (Pd) and bimetallic (Pd-Au) catalysts supported on mesoporous silica HMS, as pure and as doped with 10 wt % Ti in the hydrogenation reaction of levulinic acid [39]. The presence of gold in palladium-based catalyst, in fact, enhanced the reducibility of palladium and, by forming stable Pd-Au alloy, stabilized palladium in reduced state. The choice of Ti as a doping element was due to its promotion of chemisorption properties of metals such as Pd and Au [40]. Bimetallic systems on Ti-HMS showed the best performance, suggesting an important role played by the support. In particular, a deeper study indicated that the inserted Ti not only improves the efficiency of the bimetallic catalysts but also behaves as an active participant in the reaction mechanism.

On these premises and as a continuation of our interest on hydrogenation reaction over mono- and bimetallic catalysts [39,41], different compositions of Pd and Au nanoparticles supported on Ti doped as well as the parent mesoporous silica materials were prepared and evaluated on the hydrogenation and ring-opening of furfural. With respect to the reported literature, the purpose of this work is to investigate if and how the bimetallic Ti-doped system is able to induce the ring opening of hydrogenated furfural. The effects of Ti doping and Pd/Au ratio on the catalytic performance of Pd-Au catalysts were investigated in detail. Moreover, the influence of the support morphology was also studied by comparing two different mesostructured materials, HMS and SBA-15. The fresh and spent materials were thoroughly characterized by X-ray photoelectron spectroscopy (XPS), small angle X-ray scattering (SAXS), X-ray diffraction (XRD), N₂ adsorption isotherms (BET), high resolution transmission electron microscopy (HR-TEM), and by the temperature-programmed desorption (NH₃-TPD) in order to understand the structure–activity relations.

2. Results and Discussion

2.1. Catalytic Activity for FFR Hydrogenation

The catalytic activity of monometallic (Pd) and bimetallic (Pd-Au) catalysts, supported on ordered structured silica was investigated for the hydrogenation of FFR. As shown in Scheme 1, the reaction pathway is a cascade reaction forming several products involving into a series/ parallel hydrogenation steps.

For bimetallic catalysts on HMS, different Pd/Au atomic ratios (100:0, 75:25, 50:50, 25:75, and 0:100) were considered keeping total metal loading with a nominal value of 4%. Moreover, due to the recent investigation on Pd-Au based materials for hydrogenation reaction [39], the effect of a different morphology of the support (HMS and SBA) and the presence of Ti were studied for those bimetallic catalysts containing the same Pd/Au atomic ratio. The results of the screening of mono- and bi-metallic catalysts for FFR hydrogenation in terms of FFR conversion and the selectivity to various products are summarized in Table 1.

Table 1. Screening of mono- and bimetallic catalysts for furfural hydrogenation.

Sample	Conv. (%)	Selectivity						
		FAL	THF	THFAL	2-MF	2MTHF	1,2-PeDO	1,4-PeDO
4PdC ¹	>99	-	27	8	18	40	-	7
4PdHMS	97	31	4	31	-	-	24	10
1Pd3AuHMS	94	47	4	31	1	-	13	4
3Pd1AuHMS	98	22	2	33	2	3	29	9
2Pd2AuHMS	42	86	-	8	-	-	6	-
2Pd2AuSBA	100	5	11	30	9	12	21	12
2Pd2AuTiHMS	93	29	1	26	4	-	32	8
2Pd2AuTiSBA	97	19	6	18	3	1	40	13
4AuHMS	40	72	-	2	4	1	17	4

¹ Reaction conditions: furfural, 2.5 g; catalyst, 0.25 g; T 220 °C; H₂ 500 psi; 1000 rpm; time 5 h [9].

Under similar hydrogenation conditions used in the previous study [9], 4PdHMS gave equal selectivity towards first step FFR hydrogenation product, FAL and its subsequent hydrogenation product, THFAL, while 1,2- and 1,4-PeDO were obtained with 24 and 10% selectivity, respectively. Quite different behavior was obtained with the monometallic 4PdHMS compared to the corresponding PdC [9]. The marked difference revealed that both the nature of the support and the high dispersion of Pd in mesoporous HMS influenced the performance of the catalyst, suggesting also different reaction pathways for various products formed.

The addition of gold in varying Pd/Au ratio made a remarkable difference in the selectivity pattern. For 1Pd3AuHMS catalyst, 47% selectivity to FAL with 13% selectivity 1,2-PeDO was obtained. Very interestingly, when Pd/Au ratio was reversed as 3Pd1AuHMS, FAL selectivity dropped down to 22% with a simultaneous increase of 1,2-PeDO selectivity to 29%. For both these catalysts, THFAL selectivity remained constant in a range of 31–33%. For an equal ratio of Pd to Au catalysts (2Pd2Au) but on the two different supports HMS and SBA, a dramatic variation in 1,2-PeDO selectivity of 6% and 21%, respectively, was observed. For 2Pd2AuHMS catalyst, FAL remained the major product, but when the support was changed to SBA, higher formation of diols was achieved. However, when both the catalysts doped with Ti were used, the selectivity switched to 1,2-PeDO. At the same time, monometallic 4AuHMS catalyst showed poor activity in terms of conversion (40%) and exhibited only 17% of 1,2-PeDO selectivity. This indicated an intrinsically lower activity of gold with respect to palladium. The screening of the catalysts revealed that the insertion of Ti positively influenced the performance of the catalysts towards the formation of diols and in particular to 1,2-PeDO. For this reason, 2Pd2AuTiHMS and 2Pd2AuTiSBA catalysts were chosen for further study on optimization of reaction conditions.

The effect of the reaction temperature on the 1,2-PeDO selectivity in FFR hydrogenation was carried out in a range of 120–220 °C. For 2Pd2AuTiSBA catalyst, almost complete conversion of FFR was achieved, even at the lowest temperature of 120 °C with a selectivity in both 1,2-PeDO and FAL of 49% and 38%, respectively (Figure 1), with an increase respect to the screening reaction conditions (Table 1). With a rise in temperature to 160 °C, almost equal selectivity to FAL and 1, 2-PeDO was observed and the FFR conversion remained constant. When the temperature was further raised to 220 °C, selectivity to 1,2-PeDO decreased from 49 to 40% along with decrease in FAL selectivity from 38 to 19%. Surprisingly, 1,4-PeDO selectivity increased to 12%. This was probably due to in situ formation of levulinic acid from FAL and its conversion to 1,4-PeDO in presence of an acidic silica support [42–44]. When 2Pd2AuTiHMS was tested in the FFR hydrogenation, it was found an increment, with respect to the screening reaction conditions (Table 1) of both FFR conversion and FAL production, that was linearly dependent on the temperature. The selectivity to 1,2-PeDO (37 to 50%) increased with the rising of temperature from 120 °C to 160 °C but was found to decrease (32%) with a further rise to 220 °C. As expected, FAL selectivity was predominant (59%) at the lowest temperature (120 °C). Just to compare the effect of Ti doping on 1,2-PeDO selectivity, 2Pd2AuSBA and 2Pd2AuHMS were tested under the same conditions. While 2Pd2AuHMS catalyst did not show any significant variation in the product selectivity giving FAL as a major product (86%), 2Pd2AuSBA catalyst maintained the same 1,2-PeDO selectivity (21%) along with an increment in THFAL selectivity (30%). From these results, it could be inferred that the selectivity to 1,2-PeDO was largely influenced by both temperature (160 °C) and the presence of Ti into the catalysts. In the case of 2Pd2AuTiSBA catalyst, 49% selectivity to 1,2-PeDO was just achieved at 120 °C, while the similar results were obtained for 2Pd2AuTiHMS catalyst at 160 °C.

Concerning the effect of catalyst amount, the reaction was carried out with 0.25 g (screening condition) and 0.1 g of both Ti-doped samples for 2.5 g of furfural. In both cases, it was observed that for a lower catalyst amount of 0.1 g, independently from the temperature (160 °C), the conversion of FFR did not reach 100% producing FAL as the major product. Moreover, no improvements in the selectivity towards 1,2-PeDO diol ($\geq 20\%$) were evidenced. In all the experiments, carbon balance was found to be $>99\%$.

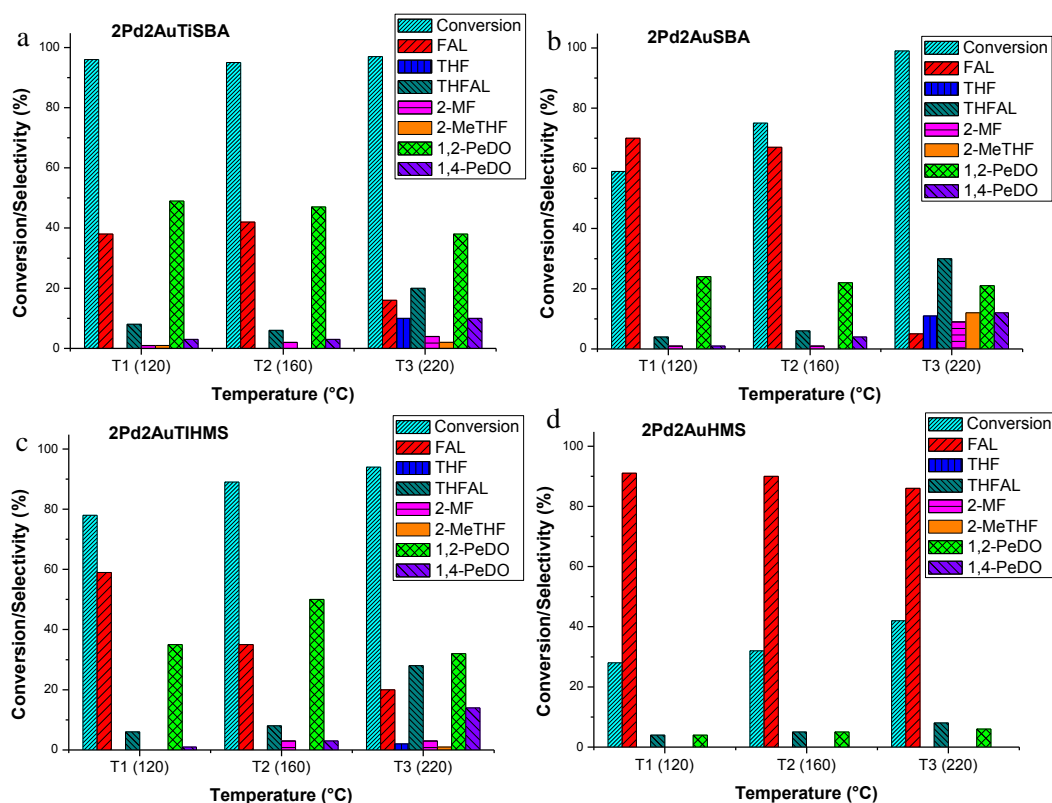


Figure 1. Effect of temperature in FFR hydrogenation over 2Pd2Au Ti-doped SBA and HMS (a,c) and un-doped (b,d) catalysts. Reaction conditions: furfural 2.5 g; catalyst 0.25 g; H₂ 500 psi; 1000 rpm; reaction time 5 h.

Figure 2 shows the effect of the reaction time on the FFR conversion and product selectivities with 0.25 g catalyst amount of bimetallic 2Pd2AuTiSBA (Figure 2a) or bimetallic 2Pd2AuSBA (Figure 2b) at 160 °C.

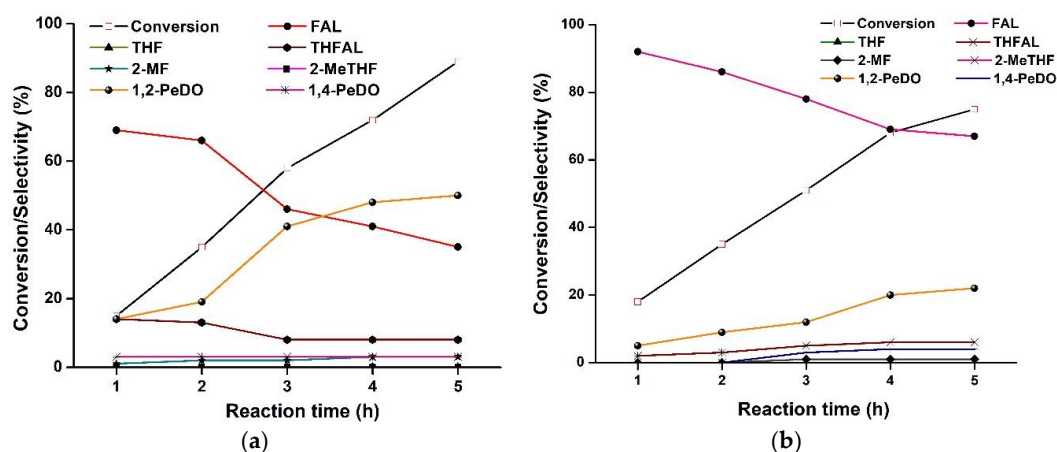


Figure 2. Conversion and selectivity vs time profiles over 2Pd2AuTi SBA (a) and 2Pd2AuSBA (b) catalysts. Reaction conditions: furfural 2.5 g; catalyst 0.25 g; temp.160 °C, H₂ 500 psi; 1000 rpm; reaction time 5 h.

As seen from Figure 2a, the conversion of FFR gradually increased from 18 to 86% with increase in reaction time from 1 to 5 h. The formation of pentanediols along with THFAL, FAL, and THF products was detected within the first hour of the reaction. Selectivity to 1,2-PeDO steadily increased

from 14% to 49% until 4 h, remaining almost constant for the next hour. At the same time, FAL and THFAL yields decreased steadily until the end of the reaction (from 69 to 35% and from 14 to 8%, respectively). A linear decrease of FAL with the simultaneous increase of 1,2-PeDO selectivity confirm that the reaction proceeds through the first step of FAL formation (Scheme 1). Furthermore, when the reaction was carried out for extended hours (10 h), there was a slight change in 1,2-PeDO selectivity (59%) at the cost of FAL product. In order to understand the role of Ti, the reaction was carried out in presence of the corresponding un-doped 2Pd2AuSBA catalyst, under the same experimental conditions. FFR conversion was quite linear and after the first hour of reaction, the main product detected was FAL, (92%) along with 1,2-PeDO (5%). As shown in Figure 2b, the conversion of FFR and the formation of 1,2-PeDO slowly proceeded until the last hour of the reaction, in which FAL was 80% with 1,2-PeDO formation up to 22%. Interestingly, both Ti-doped and un-doped samples showed poor selectivity to THF and 2-MeTHF. The effect of H₂ pressure was then investigated by carrying out the reaction in a H₂ pressure range of 100 to 750 psi in presence of 0.25 g of catalyst at 160 °C. For 2Pd2AuTiSBA catalyst, the increase of H₂ pressure had marginal effect on FFR conversion (Table 2, entries 1–4), while a predominant effect was found on the product distribution. At a lower pressure range between 100 and 300 psi, 1,2-PeDO selectivity achieved was 58–59% as a consequence of low yield of FAL (26–30%). With increase in H₂ pressure to 500 and 750 psi, the reaction showed an increase in selectivity to FAL (42%) and a decrease in selectivity to 1,2-PeDO (49%). For the 2Pd2AuTiHMS (Table 2, entries 5–8) sample, the furfural conversion was directly related to the increase in H₂ pressure (750 psi), furfural conversion was 94%. Also, in this case, when 2Pd2AuTiHMS was used, the variation of H₂ pressure mainly influenced the product selectivity nevertheless, the trend of product selectivity was quite different. With an increase in H₂ pressure from 100 to 750 psi, FAL selectivity decreased from 46% to 28%. On the contrary, 1,2-PeDO yield increased from 31 to 51% with the change of the pressure from 100 to 300 psi, while higher pressure did not further affect its selectivity. Similarly, for both 2Pd2AuSBA and 2Pd2AuHMS catalysts, selectivity to FAL was maximum for all pressures (Table 2, entries 9–12).

Table 2. Effect of H₂ pressure on FFR hydrogenation over Ti-doped catalysts.

Entry	Sample	P (psi)	Conv. (%)	Selectivity (%)				
				FAL	THFAL	2-MF	1,2-PeDO	1,4-PeDO
1		750	95	40	8	-	48	3
2	2Pd2Au	500	95	42	6	1	49	2
3	TiSBA	300	93	26	7	7	59	-
4		100	89	30	10	2	58	1
5		750	94	28	9	9	46	2
6	2Pd2Au	500	89	35	8	3	50	3
7	TiHMS	300	88	33	10	5	51	-
8		100	69	46	15	8	31	-
9	2Pd2Au	300	91	42	26	6	24	2
10	SBA	100	79	52	24	5	18	1
11	2Pd2Au	300	84	70	12	6	12	-
12	HMS	100	76	72	16	2	10	-

Reaction conditions: furfural, 2.5 g; catalyst, 0.25 g; T 160 °C; 1000 rpm; time 5 h.

Within Ti-doped SBA supported catalyst, lower H₂ pressure conditions promoted the ring opening of FAL with the formation of higher 1,2-PeDO, while, only at higher pressure did 2Pd2AuTiHMS catalyst encourage the ring opening, resulting in the formation of 1,2-PeDO. Having optimized the reaction parameters, stability and recyclability of 2Pd2AuTi-HMS/SBA catalysts were also studied, as shown in Figure 3a,b.

HMS-based catalyst was active until third use for subsequent hydrogenation reactions, showing a selectivity pattern analogous to that of the fresh catalyst. After the third reuse, the conversion decreased to 65% and a similar trend was observed both for FAL and 1,2-PeDO selectivity. In the

case of the 2Pd2AuTiSBA sample, although a slight decrease in conversion (93 to 78%) after the third recycle was observed, the selectivity to 1,2-PeDO remained constant, since the ratio of FFR conversion to 1,2-PeDO yield was the same for all cycles. Catalytic activity could be regained by rejuvenating both the catalysts with H₂. Almost similar conversion and 1,2-PeDO selectivity as the fresh run were obtained. In order to verify the stability behavior of 2Pd2AuTiSBA, the catalyst leaching test was carried out by hot filtration test. Accordingly, after 2 h, the reaction was stopped and the catalyst was separated by filtration, then the reaction mixture was continued with the filtrate devoided of catalyst. There was no change in conversion and selectivity which implied that the catalyst was quite stable and non-leachable under standard optimized reaction conditions.

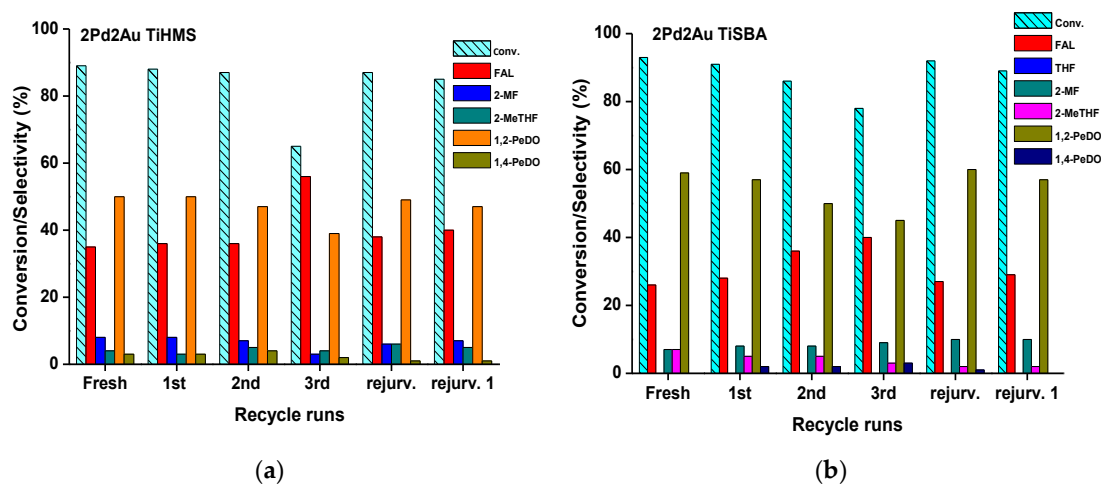


Figure 3. Catalyst recycle runs 2Pd2AuTiHMS (a) and 2Pd2AuTiSBA (b). Reaction conditions: furfural, 2.5 g; catalyst, 0.25 g; T 160 °C; H₂ 500 psi; 1000 rpm; time 5 h.

In order to understand the pathway for the formation of 1,2-PeDO in particular, if the ring-opening occurred through FAL or THFAL (see Scheme 1), some hydrogenation reactions over 2Pd2AuTiHMS and 2Pd2AuTiSBA were carried out by taking FAL and THFAL as the starting materials. When FAL was used as the starting material by using 2Pd2AuTiHMS and 2Pd2AuTiSBA as catalysts, THFAL (52% and 32% yield, respectively) and 1,2-PeDO (43% and 51% yield, respectively) were the major products for both the catalysts. On the contrary, when THFAL was employed as a starting material, for both the catalysts no hydrogenation and ring opening products were formed, indicating that THFAL was very stable under these reaction conditions.

2.2. Catalytic Characterization

The surface and structural properties of the prepared catalysts were deeply investigated by different techniques such as X-ray photoelectron spectroscopy (XPS), X-ray diffraction (XRD), N₂ adsorption isotherms (BET), Infrared spectroscopy (IR), and acid capacity measurements. Specific attention was paid to the catalysts that showed the best performance in one-pot hydrogenation and followed ring opening of furfural for the formation of 1,2-PeDO.

Small angle X-ray scattering profiles of the support materials is shown in Figure 4a,b. HMS and SBA structures are clearly evidenced for un-doped and doped silica materials. HMS shows the typical intense peak at $2\theta = 2.79^\circ$ indicative of porous structure with a regular order at 3.2 nm distance. The insertion of Ti induced a shift of the peak to lower 2θ value, indicating larger pore distance of 3.9 nm. Moreover, decrease in intensity and resolution of the peak evidenced a less ordered structure after the introduction of Ti. On the contrary, in case of SBA, no significant changes in the SAXS profile were evident with the introduction of Ti into the SBA structure. Table 3 presents the textural properties of pure HMS and SBA, as well as of those with 10% Ti. In both cases, as expected, SBA sample was

characterized by a pore to pore distance of 9.4 nm indicating larger pores size with respect to HMS. Upon insertion of titanium, the pore diameter remained unchanged in the case of HMS (2.4 nm), while it decreased in case of SBA with smaller pores in Ti-SBA (5.5 nm) with respect to parent SBA (6.2 nm). Moreover, in both cases, Ti introduction produced a thickness of the silica walls.

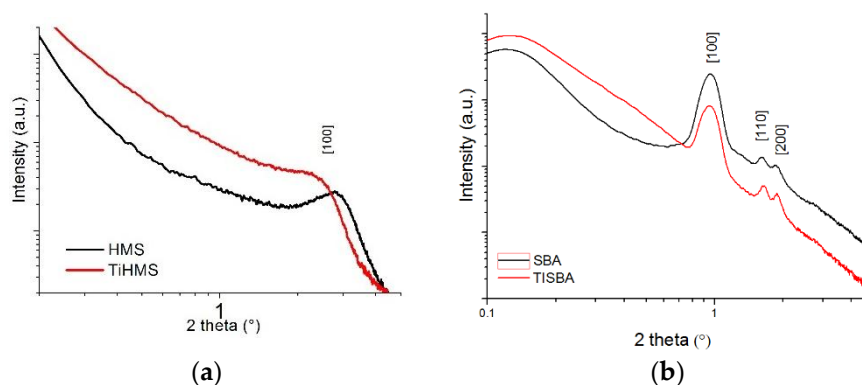


Figure 4. SAXS curves of support material HMS (a) and SBA (b) as is or Ti-doped.

Table 3. Texture properties of different support.

Sample	Pore to Pore Distance * (L, nm)	Surface Area ** (m ² g ⁻¹)	Pore Volume ** (cm ³ g ⁻¹)	Pore Diameter ** (d, nm)	Wall Thickness *** (τ, nm)
HMS	3.2	890	1.5	2.4	0.8
TiHMS	3.9	740	1.2	2.4	1.5
SBA	9.4	840	0.9	6.2	3.2
TiSBA	9.4	516	0.9	5.5	4.1

* from SAXS; ** from BET analysis; *** $\tau = L - d$.

Wide angle X-ray diffraction patterns of calcined samples are shown in Figure 5 and the results are summarized in Table 4. Palladium was present as segregated PdO and in the form of alloy with gold, for bimetallic samples. The composition of the alloy was calculated from the shift of the peaks with respect to pure metals by applying the Vegard law [45]. Interestingly, in the Titanium un-doped bimetallic catalysts, a gold rich alloy was formed along with the Au₅₀Pd₅₀ alloy and the excess of palladium was present as PdO. The insertion of Ti into the support hindered the formation of the Au-rich alloy and an almost equimolar alloy, metallic gold, and PdO were present in these samples. The particle size ranges between 5 and 15 nm with the 2Pd₂AuTiSBA sample having the smallest particles. Moreover, the 4PdHMS pattern does not contain any peaks in the XRD pattern, indicating a good dispersion of the palladium oxide particles.

Table 4. XRD derived Crystallite size and phase composition of various Pd-Au catalysts.

Sample	PdO (nm)	Au (nm)	Pd-Au (Composition)	Pd-Au (nm)
4Pd HMS	-	-	-	-
1Pd3Au HMS	15	14	-	-
3Pd1Au HMS	Traces	Traces	-	-
2Pd2Au HMS	8.5	-	Pd15Au85	15
			Pd50Au50	13
2Pd2Au SBA	8	-	Pd15Au85	10
			Pd50Au50	9
2Pd2AuTiHMS	17	18	Pd40Au60	10
2Pd2Au TiSBA	4	9	Pd57Au43	5

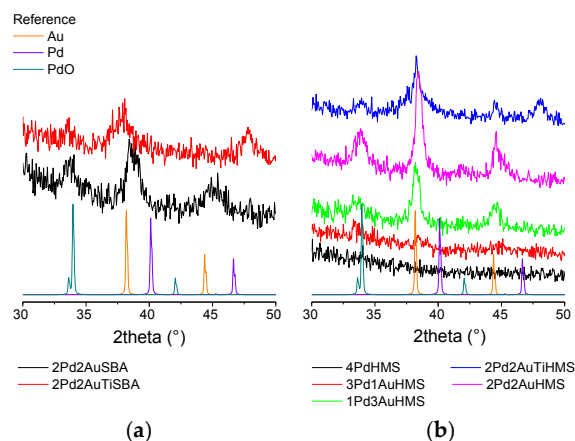


Figure 5. Wide angle XRD of Pd-Au supported on SBA (a) and HMS (b) as is or Ti-doped.

In order to obtain information about the active species on the surface, X-ray photoelectron spectroscopy analysis was performed. All binding energies were corrected by using the internal reference peak Si2p centered at 103.5 eV. Figure 6a,b shows the XPS of Pd 3d region for 2Pd2Au catalysts supported on bare and Ti-doped HMS (a) and SBA (b), respectively. All spectra contain two broad peaks separated by 5.2 eV due to the spin-orbit coupling and two components for each peak due to metallic (ca. 335 eV) and oxidized (ca. 337 eV) Palladium species, respectively, confirming the results obtained by XRD which also showed the presence of alloyed Pd and PdO. The relative amount of the two components strongly depended on the support. For the two un-doped PdAu catalysts, characterized by similar XRD patterns, the higher Pd(0)/Pd(II) ratio of 5.25 for HMS vs. 0.33 for SBA was attributed to small size alloyed particles not visible in the XRD pattern, which stabilized the elements in their metallic states with an increase in the surface concentration of Pd(0). This was confirmed by the atomic ratios of Pd/(Si + Ti) and of Au/(Si + Ti), indicating a better dispersion of metals on HMS as compared to that on SBA (Table 5). The doped samples, despite their lower surface areas with respect to those of un-doped samples, showed higher dispersion of active phase and similar Pd(0)/Pd(II) ratio, suggesting an important role of Ti in stabilizing the metallic species. Figure 6c shows the Au4f and Si2p region where, for all samples, Au4f_{7/2} binding energy corresponded to the typical B.E. of metallic gold (undistinguishable from the alloyed Au-Pd). The O1s region (not shown) presented peaks related to the corresponding supports (532 eV for SiO₂ and 529 eV for TiO₂).

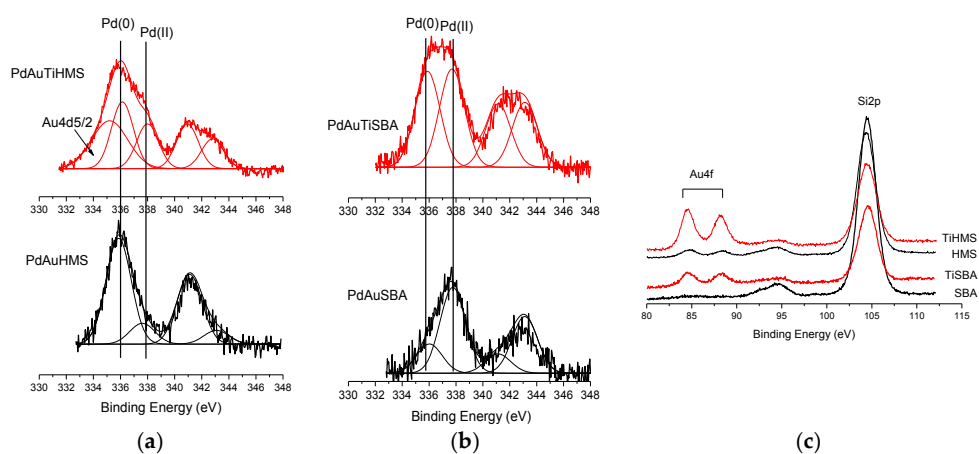
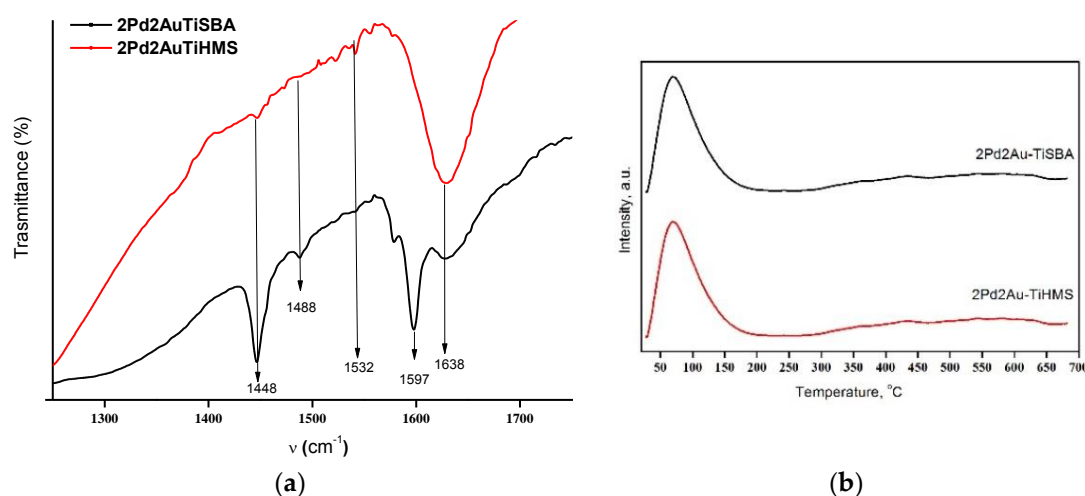


Figure 6. XPS spectra of PdAu supported silica catalysts on HMS and SBA as is or Ti-doped. (a) Pd3d on HMS/ TiHMS (b) Pd3d on SBA/TiSBA (c) Au4f and Si2p on silica supports.

Table 5. XPS data for 2Pd2Au on HMS/TiHMS or SBA/TiSBA support.

Sample	Pd3d _{5/2} eV	Au4f _{7/2} eV	Pd/(Si + Ti)	Au/(Si + Ti)	Au/Pd	Ti/Si
2Pd2Au HMS	334.9 (84%) 336.7 (16%)	83.8	0.01	0.004	0.4	-
2Pd2AuTiHMS fresh	334.7 (53%) 336.6 (47%)	83.6	0.03	0.02	0.7	0.2
2Pd2AuTiHMS Spent	334.8 (100%)	83.2	0.007	0.009	1.2	0.01
2Pd2Au SBA	336.0 (25%) 337.7 (75%)	-	0.007	-	-	-
2Pd2Au TiSBA Fresh	335.9 (49%) 337.7 (51%)	83.4	0.03	0.01	0.4	0.4
2Pd2Au TiSBA Spent	334.2 (75%) 336.4 (27%)	83.0	0.03	0.009	0.3	0.3

In order to investigate the acidic properties of Ti-doped catalysts, Py-IR and NH₃-TPD studies were carried out. (Figure 7) Analysis of Py-IR spectra allows us to establish the presence of Brønsted acidity in these materials. In both catalysts, all bands typical of different acidic sites were present but with varying intensities. For 2Pd2AuTiSBA catalyst, the absorption bands at 1448 cm⁻¹ and 1597 cm⁻¹ represented the Lewis acidity while, the bands at 1488 cm⁻¹ was due to the mixture of Lewis and Brønsted sites. The band at 1638 cm⁻¹ was attributable to the Brønsted acidity, solely. Similarly, in case of 2Pd2AuTiHMS, the bands were less intense except the band at 1532 cm⁻¹ which, once again, represented the Brønsted acidity [46]. NH₃-TPD of doped and undoped HMS as well as SBA supported bimetallic catalysts showed almost similar ammonia desorption bands between the temperature range of 0–200 °C with the higher intensity band at around 92 °C for all samples. This indicates that all catalysts possessed weak acid sites with the same strength. The quantitative acidity of SBA supported catalyst, in terms of NH₃ desorbed, was found to be 0.29 and 0.27 mmol/g for undoped and Ti-doped, respectively, while that of HMS supported catalyst was found to be 0.32 and 0.30 mmol/g for undoped and Ti-doped, respectively. The presence of medium acid sites was evident from the bands in the range of 300–600 °C. Lower acid site concentration obtained for SBA catalyst with respect to HMS catalyst and for Ti doped with respect to the corresponding undoped may be attributed to the higher dispersion of both metals on the support surface, which would cover acidic sites of the support.

**Figure 7.** Py-IR (a) and NH₃-TPD (b) spectra of 2Pd2AuTiHMS and 2Pd2AuTiSBA.

HR-TEM analysis of 2Pd2AuTi doped SBA and HMS showed an excellent dispersion of PdAu alloys on both supports (Figure 8a,b). Particle size of bimetallic PdAu alloys on Ti-HMS support was found to be in the range of 5–8 nm, while that of Pd-Au on TiSBA was in the range of 3–5 nm [47]. Crystalline nature of TiSBA supported catalyst was clearly revealed by SAED pattern (not shown), which is in a good agreement with XRD results (Table 1).

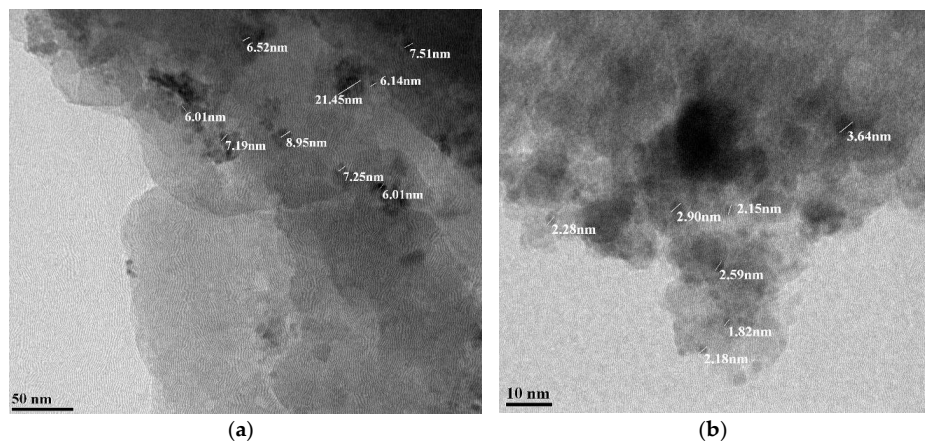


Figure 8. TEM images of (a) 2Pd2AuTiSBA and (b) 2Pd2AuTiHMS.

Finally, a structural analysis of the spent catalyst samples was also conducted to identify any changes due to the reaction cycles. Figure 9 shows the XRD patterns of these samples with small differences between the calcined and the spent catalyst samples. In both catalysts after reaction the peak related to gold alloy particles are visible whereas the PdO peaks disappear. In case of TiSBA sample, a small enlargement of the Pd₅₇Au₄₃ alloy related peak is observed. XPS spectra revealed a rather different behavior for TiHMS or TiSBA supported catalysts. Besides the increase of the metallic Pd component, the main difference regarded the surface ratio of metals over the support elements. As seen in Table 5, in TiSBA-supported sample, the atomic ratios of Pd/(Ti + Si), Au/(Pd + Si), and Ti/Si remained almost unchanged, while in the TiHMS supported catalyst, all these ratios decreased. Usually, this could be attributed to an increase of the particle size, which in this case can be excluded according to the XRD results. For these reasons, a probable collapse of the mesoporous structure occurred, resulting in masking the active metals by the silica support. The analysis of spent samples allowed explaining the different performances of the catalysts and the significant role of the support in these types of reactions.

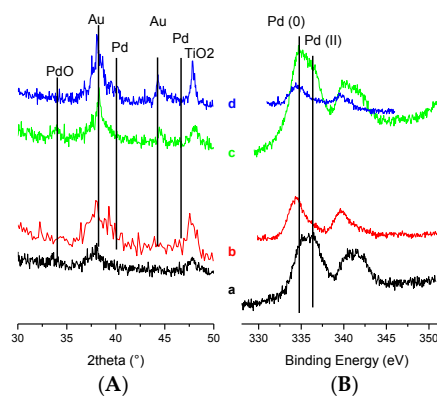
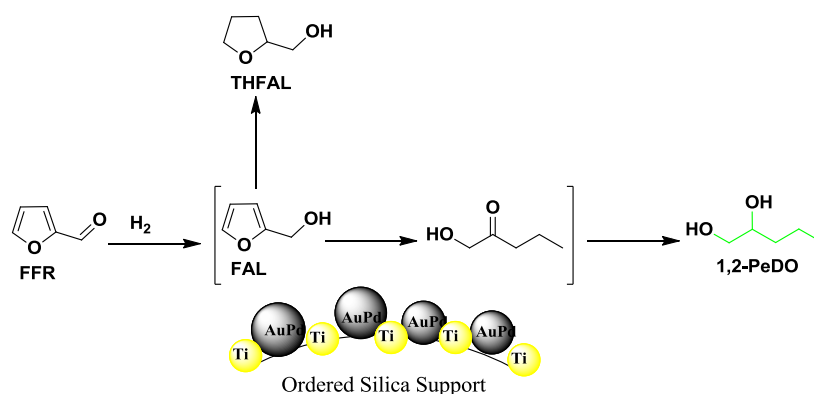


Figure 9. XRD (A) and Pd 3d XPS (B) spectra of 2Pd2AuTiSBA fresh (a) and spent (b) and 2Pd2AuTiHMS fresh (c) and spent (d).

2.3. Plausible Reaction Pathway

Taking into account all the results obtained by the catalytic activity and the characterization of the synthesised materials, a plausible reaction pathway is shown in Scheme 2, according to which 1,2-PeDO formation is possible only from the intermediate FAL. A break of C₅–O bond leads to the formation of 1-hydroxy-2-pentanone, as an intermediate, followed by its reduction [11]. Moreover, by using the bimetallic Ti-doped catalysts (2Pd2AuTi on HMS or SBA), on the basis of all kinetic and characterization results, furfural is adsorbed on palladium and gold nanoparticles where it is converted into furfuryl alcohol through reduction of formyl group. The selectivity toward 1,2-PeDO may be ascribed to two factors: the presence of alloyed Pd-Au particles of optimized ensemble size, activates H₂ molecules along with metallic gold and with a lower concentration of Brønsted sites which promote the ring opening [48,49] through the abstraction of H⁺ from FAL followed by a bond breaking at C₅–O.



Scheme 2. Plausible reaction pathway for FFR hydrogenation catalyzed by Pd-Au supported on bare and Ti doped ordered structured silica.

3. Materials and Methods

3.1. Materials

Furfural (FFR), furfuryl alcohol (FAL), tetrahydrofurfuryl alcohol (THFAL), 2-methylfuran (2-MF), 2-methyltetrahydrofuran (2-MTHF), pentanediols (PeDO), along with 1-dodecylamine, titanium iso-propoxide, and tetraethyl orthosilicate (TEOS) were purchased from Sigma Aldrich (Milan, Italy). Hydrogen was obtained from Vadilal Chemicals Pvt. Ltd (Gujarat, India).

3.2. Catalyst Preparation

3.2.1. Synthesis of Silica Supports

Both HMS and SBA-15 supports were synthesized according to a previous published procedure [50]. For the synthesis of HMS silica, TEOS (12 mL, 0.054 mol) was added to a stirring solution of ethanol (31 mL), water (31 mL), and 1-dodecylamine (3.68 mL, 0.016 mol). The mixture was stirred at room temperature for 24 h. The white precipitate obtained was filtered under vacuum and washed with deionised water (36 mL) and ethanol (36 mL). The solid was dried overnight at room temperature and then calcined at 600 °C for 4 h with a ramp of 5 °C/min. The SBA-15 silica was prepared by using a non-ionic amphiphilic triblock polymer, Pluronic P123, as a surfactant. The polymer (8.1 g) was dissolved in deionised water (146.8 mL) and conc. HCl (37 v %, 4.4 g) and stirred overnight at 35 °C in a 250 mL one neck flask. TEOS (17.1 mL, 0.077 mol) was quickly added to this solution and stirred for 24 h at 35 °C. The milky suspension was aged at 100 °C for 24 h in a closed polypropylene bottle. The solid product was filtered, washed with HCl/water mixture, and calcined in air at 500 °C for 5 h (ramp of 10 °C/min).

3.2.2. Synthesis of Ti-HMS and Ti-SBA

The titanium containing meso-structured HMS and SBA-15 with composition of 10 wt % of TiO₂ and 90 wt % silica (labeled as TiHMS and TiSBA, respectively) were synthesized by grafting methodologies [39]. In typical procedure, Ti(iOPr)₄ (1.67 mL) was added to a stirred suspension of silica support (2.7 g) in toluene (100 mL). The mixture was refluxed for 24 h at 110 °C. The material was then recovered by filtration, washed several times with toluene, dried, and then calcined at 500 °C for 4 h.

3.2.3. Preparation of the Pd_xAu_y Bimetallic Nanoparticles Supported on Mesoporous Silica

The monometallic Pd and the bimetallic Pd-Au catalysts with different Pd/Au atomic ratios (100:0, 75:25, 50:50, and 25:75) were prepared by deposition–precipitation method following the procedure adopted previously [39]. All the catalysts were prepared with a total metal loading of 4 wt%. According to this procedure, urea in a molar ratio of 4:1 with respect to the metals, was added to an aqueous suspension of the support containing dissolved precursor salts PdCl₂ and HAuCl₄·3H₂O in the appropriate amount. By heating to 90 °C, the urea decomposed generating a basic solution, induces the precipitation of metal hydroxides on the surface of the support. Then the solution having pH of ~8, was kept under reflux with stirring for 8 h. The suspension was filtered, washed with distilled water, and dried at 60 °C. The catalysts were, then, calcined at 400 °C for 2 h. Before being used in the hydrogenation reactions, catalysts were reduced in a fixed bed reactor under H₂ flow at 300 °C with a heating rate of 2 °C/min during 3 h.

3.3. Catalyst Characterization

The X-ray diffraction measurements were performed with a Bruker goniometer (Bruker AXS, Karlsruhe, Germany) using Ni-filtered Cu K α radiation. A proportional counter and 0.05° step sizes in 2 θ were used. The assignment of the crystalline phases was based on the JPDFS powder diffraction file cards. Small Angle X-ray scattering (SAXS) was performed with BRUKER AXS NANOSTAR with step sizes of 0.02° in 2 θ .

X-ray photoelectron spectroscopy (XPS) analyses were performed with a VG Microtech ESCA 3000 Multilab (VG Scientific, Sussex, UK), equipped with a dual Mg/Al anode. The spectra were excited by the un-monochromatized Al K α source (1486.6 eV) run at 14 kV and 15 mA. The analyzer operated in the constant analyzer energy (CAE) mode. For the individual peak energy regions, a pass energy of 20 eV set across the hemispheres was used. Survey spectra were measured at 50 eV pass energy. The sample powders were analyzed as pellets, mounted on a double-sided adhesive tape. The pressure in the analysis chamber was of the order of 10–8 torr during data collection. The constant charging of the samples was removed by referencing all the energies to the Si 2p set at 103.5 eV. The invariance of the peak shapes and widths at the beginning and at the end of the analyses ensured absence of differential charging. Analyses of the peaks were performed with the software provided by VG (version 2.3.17, Casa Software Ltd. Wilmslow, Cheshire, UK, 2009), based on non-linear least squares fitting program using a weighted sum of Lorentzian and Gaussian component curves after background subtraction [51,52]. Atomic concentrations were calculated from peak intensity using the sensitivity factors provided with the software. The binding energy values are quoted with a precision of ± 0.15 eV and the atomic percentage with a precision of $\pm 10\%$.

HR-TEM images of the catalyst were obtained using transmission electron microscope model JEOL 1200 EX (JEOL, Tokyo, Japan). For this purpose, a small amount of the solid sample was sonicated in 2-propanol for 10 min. A drop of the prepared suspension was deposited on a Cu grid coated with a carbon layer, and the grid was then dried at room temperature before analysis.

The Elemental analysis of metals (Pd, Au) in the powders was performed by Microwave Plasma-Atomic Emission Spectroscopy (MP-AES) (Agilent, CA, USA) using a 4200 MP-AES system from Agilent and the results are agree with the nominal values. The powder (ca. 10 mg) was dissolved

in 2 mL of aqua regia at 70 °C. Then the volume was increased up to 10 mL with distilled water and the solution was analyzed.

The textural properties were obtained using a Carlo Erba Sorptomat 1900 instrument (Fisons, UK). The fully computerized analysis of the N₂ adsorption isotherm at 77 K allowed obtaining, through the BET method in the standard pressure range 0.05–0.3 P/P₀, the specific surface areas of the samples. The total pore volume, V_p, was evaluated on the basis of the amount of nitrogen adsorbed at a relative pressure of 0.998, while mesopore size distribution values and mesopore volumes were calculated by applying BJH model in the range of P/P₀ of 0.1–0.98.

Py-IR spectra were recorded on a Spectrum 2000 Perkin Elmer instrument (Perkin Elmer Singapore) by using KBR pellet as background.

Temperature-programmed desorption of ammonia (NH₃-TPD) was performed on Micromeritics Chemisorbs 2720 instrument (Micromeritics, Norcross, GA, USA). In a typical experiment, 0.05 g of catalyst was taken in a U-shaped, flow-through, quartz sample tube. Prior to measurements, the catalyst was pre-treated in He (25 cm³/min) at 200 °C for 2 h. the mixture of NH₃ in He (30%) was passed (25 cm³/min) at 50 °C for 1 h. The TPD measurements were carried out in the range 50 to 700 °C with a heating rate of 10 °C/min. Ammonia concentration in the effluent was monitored with a gold-plated filament thermal conductivity detector.

3.4. Catalytic Hydrogenation of Furfural

Catalytic hydrogenation of furfural was performed in a 300 mL stainless steel autoclave equipped with overhead stirrer, a pressure gauge, and automatic temperature control facility. In a typical experiment, 2.5 g furfural in 95 mL solvent (IPA) and catalyst (0.25 g) were charged into the reactor. It was then sealed and purged with N₂ for 2 times to exclude air and then by H₂. After attaining the desired reaction temperature, the reactor was pressurized with hydrogen at 500 psi and the reaction was started by stirring the contents at 1000 rpm. 1 mL of the liquid samples was withdrawn from the reactor for GC analysis, with 1 h time interval each for monitoring the progress of the reaction. H₂ consumption as a function of time was also recorded and the reaction was carried out at almost constant pressure by filling it with fresh H₂ as per the consumption.

Liquid samples collected from time to time were analyzed using Thermo TRACE 700 GC (Thermo Fisher Scientific, India) equipped with HP-5 capillary column having the dimensions, 30 m × 0.32 mm × 0.25 μm, and a flame ionization detector (Thermo Fisher Scientific, India). 1 μL of sample was analyzed by gas-chromatography according to the temperature program: 40 °C (3 min), 10 °C/min, 45 °C (1 min), 100 °C/min, 60 °C (0 min), 200 °C/min, and 250 °C (1 min). Performance of mono and bimetallic systems was evaluated in terms of FFR conversion (%) and product selectivity (%) as defined below experimental details.

$$\% \text{Conversion} = \frac{\text{Moles of furfural consumed}}{\text{Initial moles of furfural}} \times 100 \quad \% \text{Selectivity} = \frac{\text{Moles of product formed}}{\text{Total moles of product formed}} \times 100$$

Recycling experiments were performed over the most active catalysts of the series, 2Pd2AuTiHMS and 2Pd2AuTiSBA. After the reaction, the crude was separated by settling of the catalyst. The reactor was recharged by fresh reaction mixture for the subsequent cycles. Rejuvenation of deactivated catalysts was done by reducing it with H₂ flow with the same protocol used previously during catalyst preparation. Solvent recycling was carried out by its recovery by distillation of the reaction crude after each subsequent run.

4. Conclusions

In this study, different Pd-Au bimetallic catalysts supported on bare and Ti-doped ordered structured silica were used for one-pot hydrogenation of furfural to achieve the open chain product, 1,2-pentadiol. The relationship between the structural features and the activity of the materials

was investigated to understand the ring opening pathway in this cascade hydrogenation reaction. In particular, Pd/Au molar ratio, the introduction of Ti, and the different morphology of the support (HMS or SBA) were studied. Among the various catalysts, 2Pd2Au on Ti doped SBA presented the best performance with very high furfural conversion of 93% and the highest selectivity of 59% to 1,2-pentanediol. It was found that the insertion of Ti into structured silica improve the ring opening pathway towards the formation of pentanediol. Moreover, in terms of stability of the material, the SBA derived samples resulted more stable due to its morphology that avoid any leaching of active site and maintain the mesoporous structure, suggesting an important role played by the support itself. A plausible reaction pathway is suggested in which bimetallic Pd-Au alloy and Ti species cooperate together to the formation of ring opened products instead of ring hydrogenated and side chain hydrogenated products.

Finally, by the choice of an appropriate bimetallic catalyst and support system combined with the reaction conditions, it was possible to switch the selectivity towards the ring opening pathway or the selective hydrogenated cyclic.

Author Contributions: This study was conducted through contributions of all authors. C.V.R and M.L.T designed the study and wrote the paper. M.L.T., V.L.P. and N.S.D. designed and performed the experiments and analyzed the data.

Funding: This research received no external funding.

Acknowledgments: N.S.D. gratefully acknowledges Department of Science and Technology (DST) New Delhi, for financial support to him.

Conflicts of Interest: The authors declare no conflict of interest.

References

1. Chheda, J.; Huber, G.W.; Dumesic, J.A. Liquid-phase catalytic processing of biomass-derived oxygenated hydrocarbons to fuels and chemicals. *Angew. Chem. Int. Ed.* **2007**, *46*, 7164–7183. [[CrossRef](#)] [[PubMed](#)]
2. Corma, A.; Iborra, S.; Velty, A. Chemical routes for the transformation of biomass into chemicals. *Chem. Rev.* **2007**, *107*, 2411–2502. [[CrossRef](#)] [[PubMed](#)]
3. Fernando, S.; Adhikari, S.; Chandrapal, C.; Murali, N. Current Status, Challenges, and Future Direction. *Energy Fuels* **2006**, *20*, 1727–1737. [[CrossRef](#)]
4. Cortright, R.D.; Davda, R.R.; Dumesic, J.A. Hydrogen from catalytic reforming of biomass-derived hydrocarbons in liquid water. *Nature* **2002**, *418*, 964–967. [[CrossRef](#)] [[PubMed](#)]
5. Rodiansono, R.; Khairi, S.; Hara, T.; Ichikuni, N.; Shimazu, S. Highly efficient and selective hydrogenation of unsaturated carbonyl compounds using Ni–Sn alloy catalysts. *Catal. Sci. Technol.* **2012**, *2*, 2139–2145. [[CrossRef](#)]
6. Martinez-Garcia, A.; Ortiz, M.; Martinez, R.; Ortiz, P.; Reguera, E. The condensation of furfural with urea. *Ind. Crop. Prod.* **2004**, *19*, 99–106. [[CrossRef](#)]
7. Biradar, N.S.; Hengne, A.M.; Birajdar, S.N.; Niphadkar, P.S.; Joshi, P.N.; Rode, C.V. Single-Pot Formation of THFAL via Catalytic Hydrogenation of FFR over Pd/MFI Catalyst. *ACS Sustain. Chem. Eng.* **2014**, *2*, 272–281. [[CrossRef](#)]
8. Date, N.S.; Hengne, A.M.; Haung, K.-W.; Chikate, R.C.; Rode, C.V. Single pot Selective hydrogenation of furfural to 2-methylfuran over carbon supported iridium catalysts. *Green Chem.* **2018**, *20*, 2027–2037. [[CrossRef](#)]
9. Date, N.S.; Biradar, N.S.; Chikate, R.C.; Rode, C.V. Effect of reduction Protocol of Pd Catalysts on Product Distribution in Furfural Hydrogenation. *Chem. Sel.* **2017**, *2*, 24–32. [[CrossRef](#)]
10. Xu, W.; Wang, H.; Liu, X.; Ren, R.; Wang, Y.; Lu, G. Direct catalytic conversion of furfural to 1,5-pentanediol by hydrogenolysis of the furan ring under mild conditions over Pt/Co₂AlO₄ catalyst. *Chem. Commun.* **2011**, *47*, 3924–3926. [[CrossRef](#)] [[PubMed](#)]
11. Mizugaki, T.; Yamakawa, T.; Nagatsu, Y.; Maeno, Z.; Mitsudome, T.; Jitsukawa, K.; Kaneda, K. Direct Transformation of furfural to 1,2-pentadiol using hydrotalcite-supported platinum nanoparticle catalyst. *ACS Sustain. Chem. Eng.* **2014**, *2*, 2243–2247. [[CrossRef](#)]

12. Ma, R.; Wu, X.P.; Tong, T.; Shao, Z.J.; Wang, Y.; Liu, X.; Xia, Q.; Gong, X. The Critical Role of Water in the Ring Opening of Furfural Alcohol to 1,2-Pentanediol. *ACS Catal.* **2017**, *7*, 333–337. [[CrossRef](#)]
13. Nakamura, H.; Taniguchi, Y. Printing Method and Printed Products. JP Patent 201236121, 23 February 2012.
14. Siegmeier, R.; Prescher, G.; Maurer, H.; Hering, G. Continuous Process for the Production of 1,2-Pentanediol. U.S. Patent 4,605,795, 12 August 1986.
15. Koch, O.; Koeckritz, A.; Kant, M.; Martin, A.; Schoening, A.; Armbruster, U.; Bartoszek, M.; Evert, S.; Lange, B.; Bienert, R. U.S. Method for Producing 1,2-Pentanediol. U.S. Patent 8,921,617, 30 December 2014.
16. Koso, S.; Furikado, I.; Shima, A.; Miyazawa, T.; Kunimori, K.; Tomishige, K. Chemoselective hydrogenolysis of tetrahydrofurfuryl alcohol to 1,5-pentanediol. *Chem. Commun.* **2009**, *15*, 2035–2037. [[CrossRef](#)] [[PubMed](#)]
17. Nakagawa, Y.; Tomishige, K. Production of 1,5-pentanediol from biomass via furfural and tetrahydrofurfuryl alcohol. *Catal. Today* **2012**, *195*, 136–143. [[CrossRef](#)]
18. Bel'skii, I.F.; Shuikin, N.I.; Shostakovskii, V.M. Effect of carbonyl and alkoxy carbonyl groups on the hydrogenolysis of the furan ring under the conditions of vapor-phase hydrogenation. *Bull. Acad. Sci. USSR* **1962**, *11*, 1727–1730. [[CrossRef](#)]
19. Winnick, C.N. Preparation of Glycols and Glycol Ethers. U.S. Patent 3,475,499, 28 October 1969.
20. Hambrack, K.O.; Roberbson, J.A. Production of 1, 5-pentanediol from Furfural. U.S. Patent 2,768,979, 30 October 1956.
21. Shokouhimehr, M. Magnetically separable and sustainable nanostructured catalysts for heterogeneous reduction of nitroaromatics. *Catalysts* **2015**, *5*, 534–560. [[CrossRef](#)]
22. Aejung, K.; Mahdi, S.; Shahrouz, A.; Shokouhimehr, M. Palladium nanocatalysts confined in mesoporous silica for heterogeneous reduction of nitroaromatics. *Energy Environ. Focus* **2015**, *4*, 18–23.
23. Nguyen, C.; Kim, J.; Yoon, S.; Yang, E.; Kwak, J.; Lee, M.; An, K. Supported Pd nanoparticles catalysts with high activities and selectivities in liquid-phase furfural hydrogenation. *Fuel* **2018**, *226*, 607–617. [[CrossRef](#)]
24. Chen, J.; Ge, Y.; Guo, Y.; Chen, J. Selective hydrogenation of biomass-derived 5-hydroxymethylfurfural using palladium catalyst supported on mesoporous graphitic carbon nitride. *J. Energy Chem.* **2018**, *27*, 283–289. [[CrossRef](#)]
25. Ouyang, W.; Yopez, A.; Romero, A.; Luque, R. Towards industrial furfural conversion: Selectivity and stability of palladium and platinum catalysts under flow regime. *Catal. Today* **2018**, *308*, 32–37. [[CrossRef](#)]
26. Albilali, R.; Douthwaite, M.; He, Q.; Taylor, S. The selective hydrogenation of furfural over supported palladium nanoparticle catalysts prepared by sol-immobilisation: Effect of catalyst support and reaction conditions. *Catal. Sci. Technol.* **2018**, *8*, 252–267. [[CrossRef](#)]
27. Wang, C.; Liu, Z.; Wang, L.; Dong, X.; Zhang, J.; Wang, G.; Han, S.; Meng, X.; Zheng, A.; Xiao, F. Importance of zeolite wettability for selective hydrogenation of furfural over Pd@zeolite catalysts. *ACS Catal.* **2018**, *8*, 474–481. [[CrossRef](#)]
28. Srivastava, S.; Jadeja, G.C.; Parikh, J. Synergim studies on alumina-supported copper-nickel catalysts towards furfural and 5-hydroxymethylfurfural hydrogenation. *J. Mol. Catal. A Chem.* **2017**, *426*, 244–256. [[CrossRef](#)]
29. Yang, Y.; Liu, Q.; Li, D.; Tan, J.; Zhang, Q.; Wang, C.; Ma, L. Selective hydrodeoxygenation of 5-hydroxymethylfurfural to 2,5-dimethylfuran on Ru-MoO_x/C catalysts. *RSC Adv.* **2017**, *7*, 16311–16318. [[CrossRef](#)]
30. Nakagawa, Y.; Takada, K.; Tamura, M.; Tomishige, K. Total hydrogenation of furfural and 5-hydroxymethylfurfural over supported Pd-Ir alloy catalyst. *ACS Catal.* **2014**, *4*, 2718–2726. [[CrossRef](#)]
31. Liu, S.; Amada, Y.; Tamura, M.; Nakagawa, Y.; Tomishige, K. One-pot selective conversion of furfural into 1,5-pentanediol over a Pd-added Ir-ReO_x/SiO₂ bifunctional catalyst. *Green Chem.* **2014**, *16*, 617–626. [[CrossRef](#)]
32. Li, S.; Wang, Y.; Gao, L.; Wu, Y.; Yang, X.; Sheng, P.; Xiao, G. Short channeled Ni-Co/SBA-15 catalysts for highly selective hydrogenation of biomass-derived furfural to tetrahydrofurfuryl alcohol. *Microporous Mesoporous Mater.* **2018**, *262*, 154–165. [[CrossRef](#)]
33. Nishimura, S.; Ikeda, N.; Ebitani, K. Selective hydrogenation of biomass-derived 5-hydroxymethylfurfural (HMF) to 2,5-dimethylfuran (DMF) under atmospheric hydrogen pressure over carbon supported PdAu bimetallic catalyst. *Catal. Today* **2014**, *232*, 89–98. [[CrossRef](#)]
34. Zhang, F.; Liu, Y.; Yuan, F.; Niu, X.; Zhu, Y. Efficient Production of the liquid fuel 2,5-dimethylfuran from 5-hydroxymethylfurfural in the absence of acid additive over bimetallic PdAu supported on Graphitized Carbon. *Energy Fuels* **2017**, *31*, 6364–6373. [[CrossRef](#)]

35. La Parola, V.; Testa, M.L.; Venezia, A.M. Pd and PdAu catalysts supported over 3-MPTES grafted HMS used in the HDS of thiophene. *Appl. Catal. B Environ.* **2012**, *119*, 248–255. [[CrossRef](#)]
36. Yang, X.; Chen, D.; Liao, S.; Song, H.; Li, Y.; Fu, Z.; Su, Y. High-performance Pd–Au bimetallic catalyst with mesoporous silica nanoparticles as support and its catalysis of cinnamaldehyde hydrogenation. *J. Catal.* **2012**, *291*, 36–43. [[CrossRef](#)]
37. Ottoni, C.A.; Da Silva, S.G.; De Souza, R.F.B.; Neto, A.O. Glycerol oxidation reaction using PdAu/C electrocatalysts. *Ionics* **2016**, *22*, 1167–1175. [[CrossRef](#)]
38. Schwarz, T.J.; Lyman, S.D.; Motagamwala, A.H.; Mellmer, M.A.; Dumesic, J.A. Selective Hydrogenation of Unsaturated Carbon–Carbon Bonds in Aromatic-Containing Platform Molecules. *ACS Catal.* **2016**, *6*, 2047–2054. [[CrossRef](#)]
39. Testa, M.L.; Demailly, L.C.; La Parola, V.; Venezia, A.M.; Pinel, C. Effect of Au on Pd supported over HMS and Ti doped HMS as catalysts for the hydrogenation of levulinic acid to γ -valerolactone. *Catal. Today* **2015**, *257*, 291–296. [[CrossRef](#)]
40. Ko, C.S.; Gorte, R.J. A study of surface defect of Si (511) by RHEED and LEED. *Surf. Sci.* **1985**, *161*, 597–607. [[CrossRef](#)]
41. Date, N.S.; Chikate, R.C.; Roh, H.S.; Rode, C.V. Bifunctional role of Pd/MMT-K 10 catalyst in direct transformation of furfural to 1,2-pentanediol. *Catal. Today* **2018**, *309*, 195–201. [[CrossRef](#)]
42. Mellmer, M.; Gallo, J.; Alonso, D.; Dumesic, J. Selective Production of Levulinic Acid from Furfuryl Alcohol in THF Solvent Systems over H-ZSM-5. *ACS Catal.* **2015**, *5*, 3354–3359. [[CrossRef](#)]
43. Hengne, A.M.; Kamble, S.B.; Rode, C.V. Single pot conversion of furfuryl alcohol to levulinic esters and γ -valerolactone in the presence of sulfonic acid functionalized ILs and metal catalysts. *Green Chem.* **2013**, *15*, 2540–2557. [[CrossRef](#)]
44. Li, M.; Li, G.; Li, N.; Wang, A.; Dong, W.; Wang, X.; Conga, Y. Aqueous phase hydrogenation of levulinic acid to 1,4-pentanediol. *Chem. Commun.* **2014**, *50*, 1414–1416. [[CrossRef](#)] [[PubMed](#)]
45. West, A.R. *Solid State Chemistry and Its Applications*; Wiley: Chichester, UK, 1998.
46. Barzetti, T.; Selli, E.; Moscotti, D.; Forni, L. Pyridine and ammonia as probes for FTIR analysis of solid acid catalysts. *J. Chem. Soc. Faraday Trans.* **1996**, *92*, 1401–1407. [[CrossRef](#)]
47. Lim, B.; Kobayashi, H.; Yu, T.; Wang, J.; Kim, M.J.; Li, Z.Y.; Rycemga, M.; Xia, Y. Synthesis of Pd–Au Bimetallic Nanocrystals via Controlled Overgrowth. *J. Am. Chem. Soc.* **2010**, *132*, 2506–2507. [[CrossRef](#)] [[PubMed](#)]
48. Santi, D.; Holl, T.; Calemna, V.; Weitkamp, J. High-performance ring-opening catalysts based on iridium-containing zeolite Beta in the hydroconversion of decalin. *Appl. Catal. A Gener.* **2013**, *455*, 46–57. [[CrossRef](#)]
49. Miedziak, P.J.; Edwards, J.K.; Taylor, S.H.; Knight, D.W.; Tarbit, B.; Hutchings, G.J. Gold as a Catalyst for the Ring Opening of 2,5-Dimethylfuran. *Catal. Lett.* **2018**. [[CrossRef](#)]
50. Testa, M.L.; Tummino, M.L.; Agostini, S.; Avetta, P.; Deganello, F.; Montoneri, E.; Magnacca, G.; Prevot, A.B. Synthesis, characterization and environmental application of silica grafted photoactive substances isolated from urban biowaste. *RSC Adv.* **2015**, *5*, 47920–47927. [[CrossRef](#)]
51. Shirley, D.A. High-Resolution X-ray Photoemission Spectrum of the Valence Bands of Gold. *Phys. Rev. B* **1972**, *5*, 4709–4715. [[CrossRef](#)]
52. Sherwood, P.M.A.; Briggs, D.; Seah, M.P. (Eds.) *Practical Surface Analysis*; Wiley: New York, NY, USA, 1990; pp. 181–185.

